

Optomechanics based on angular momentum exchange between light and matter

H. Shi

Department of Physics, G07 Physical Sciences Building, Cornell University, Ithaca, NY 14853, USA

E-mail: hxs673@cornell.edu

M. Bhattacharya

School of Physics and Astronomy, Rochester Institute of Technology, 84 Lomb Memorial Drive, Rochester, NY 14623, USA

E-mail: mxbps@rit.edu

Abstract. The subject of optomechanics involves interactions between optical and mechanical degrees of freedom, and is currently of great interest as an enabler of fundamental investigations in quantum mechanics, as well as a platform for ultrasensitive measurement devices. The majority of optomechanical configurations rely on the exchange of linear momentum between light and matter. We will begin this tutorial with a brief description of such systems. Subsequently, we will introduce optomechanical systems based on *angular* momentum exchange. In this context, optical fields carrying polarization and orbital angular momentum will be considered, while for the mechanics, torsional and free rotational motion will be of relevance. Our overall aims will be to supply basic analyses of some of the existing theoretical proposals, to provide functional descriptions of some of the experiments conducted thus far, and to consider some directions for future research. We hope this tutorial will be useful to both theorists and experimentalists interested in the subject.

PACS numbers: 42.50.Pq, 42.60.Da, 42.50.Ct, 42.50.Dv

1. Introduction

Optomechanical systems, which are based on the interaction between optical and mechanical degrees of freedom, are currently under intense research focus [1, 2, 3, 4, 5, 6, 7, 8, 9, 10, 11, 12, 13]. Much of the interest in these systems is due to their ability to access quantum mechanics at more macroscopic scales than ever before. For example, a major accomplishment of the field has been the cooling of a microfabricated harmonic oscillator, consisting of roughly 10^{11} atoms, to its quantum mechanical ground state [14]. Optomechanical systems therefore provide an avenue for investigating fundamental quantum mechanical issues such as wave function collapse [15, 16], superposition [17, 18], decoherence [19], entanglement [20, 21], backaction [22] and Planck-scale physics [23]. Furthermore, these optomechanical systems hold great potential as platforms for ultrasensitive measurement technologies. Indeed, optomechanical principles underlie cutting-edge displacement [24] and force [25, 26] sensors, phonon detectors [27, 28], gravitational wave interferometers [7], thermometers [29], accelerometers [30], and magnetometers [31], to cite a few examples. While a variety of physical configurations are used in the investigations mentioned above, in almost all of them, the optical and mechanical degrees of freedom interact via the exchange of *linear* momentum.

However, light can also exchange *angular* momentum with matter [32, 33, 34, 35, 36, 37, 38, 39, 40, 41, 42, 43]. Since the pioneering experiment of Beth, it has been known that light can carry spin angular momentum (i.e. polarization), which in turn can exert torque on bulk matter [44, 45]. Subsequently, a seminal paper by Allen et al. in 1992 pointed out that photons could also carry orbital angular momentum (OAM), encoded as spatial structure in the transverse profile of the corresponding optical beam [46, 47]. Unlike spin, which can only take values $s = \pm\hbar$, photonic OAM can take any value $l = 0, \pm\hbar, \pm2\hbar, \dots$. Of importance to this tutorial is the fact that OAM-carrying beams can exert torque on matter as well, with experiments demonstrating optical rotation effects on nanoparticles [48, 49, 50], liquid crystals [51], and Bose-Einstein condensates [52, 53, 54], for example. Also of relevance is the fact that, due to their intrinsic spatial inhomogeneities, beams with OAM can sense the circulation of material particles, via the rotational Doppler shift [55, 56]. This has been verified in velocimetry experiments [50, 57, 58, 59] (which have also been implemented with circularly polarized beams [60]). Further, it is relevant to mention that the practically infinite Hilbert space corresponding to the virtually unlimited OAM available per photon has proved to be an important resource for quantum information processing [61, 62, 63, 64, 65, 66, 67, 68, 69, 70, 71]. Lastly, OAM carried by an optical beam is associated with the presence of singularities, i.e. vortices, in the beam profile. These structures have their own interesting dynamics and place OAM-carrying beams into the larger arena of ‘singular optics’ [72, 73, 74, 75]. There are many other applications of OAM-carrying beams; we have mainly mentioned those which are relevant to our discussion.

This tutorial aims to introduce optomechanical systems which are based on angular momentum exchange between light and matter. For the optical fields, this

will imply the consideration of photons carrying either polarization or OAM. For the mechanics, torsional and free rotational motion will be of importance. To our knowledge, existing introductions to, and reviews of, the micromanipulation of matter with angular momentum-carrying beams largely deal with liquid media [76, 77, 78, 79]. In contrast, the present tutorial will consider instead only systems under vacuum. With few exceptions, we will consider beams carrying well-defined optical angular momentum per photon, and will neglect the effects of linear photonic momentum on mechanical torsional or free rotational motion [80, 81, 82, 83].

It is worth stating explicitly the interest behind considering the two types of mechanical motion mentioned above. Torsional oscillators are often the instruments of choice for precision measurement experiments. For example, they were used in historic measurements of the static electric force by Coulomb [84], of the gravitational force by Cavendish [85], and of optical polarization by Beth [44]. Furthermore, a key difference between linear and torsional oscillations is that the linear vibrational motion of an object is affected by its total mass, while the torsional oscillations are affected not only by the total mass but also by how that mass is distributed, i.e. by the moment of inertia. For example, the mass of a sphere of radius r varies as r^3 , but the moment of inertia goes as r^5 . Thus, smaller objects are easier to move linearly, but even easier to move torsionally. These distinctions make it worthwhile to study torsional oscillations on their own.

On the other hand, free mechanical rotation presents some entirely novel features, compared to linear or torsional oscillatory motion, especially in the quantum regime. For example, it is well known that since the harmonic oscillator is a linear system (i.e. its equations of motion are linear in the dynamical variables, or equivalently, the energy eigenvalues are evenly spaced), quantum effects are quite difficult to observe. In other words, the quantum oscillator behaves, for the most part, like a classical oscillator. To observe quantum effects, one usually needs to introduce some sort of nonlinear interaction, for example, by coupling the oscillator to the mode of an electromagnetic field, or to a two-level system [11]. The free rotor, in contrast, is a nonlinear system (i.e. its equations of motion are nonlinear in the dynamical variables, or equivalently, its energy spectrum is anharmonic, see below), which suggests that it might be easier to observe quantum effects in its behavior without the use of any auxiliary systems. One such quantum effect, which would be interesting to verify at much larger than atomic mass scales, is the quantization of angular momentum, one of the central predictions of quantum mechanics [86]. A second intriguing feature of the rotor is that, unlike the harmonic oscillator (and other elementary quantum systems such as the square well, the delta function well, or the Morse potential), it has no ground state energy [86]. This can be seen from the Hamiltonian of a particle of mass m rotating in a circle of radius r ,

$$H_r = \frac{L_z^2}{2I}, \quad (1)$$

where L_z is the angular momentum of the particle, and

$$I = mr^2, \quad (2)$$

is its moment of inertia. The eigenvalues of H_r are $l^2\hbar^2/2I, l = 0, 1, 2, \dots$. Thus, the ground state ($l = 0$) is perfectly rotationless. Finally, the prospect of observing counter-rotating superpositions of mechanically rotating states [87] is quite tantalizing, and is the neutral mechanical analog of counter-propagating persistent electronic currents in superconducting circuits [89]. From a more practical point of view, freely rotating mechanical systems could possibly be used for gyroscopy [50] and for storing photonic OAM [87]. Conversely, optical beams carrying OAM could be used to probe mechanical rotation, in a quantum-limited manner [88].

The remainder of the tutorial is organized in the following way. We first introduce optomechanics based on electromagnetic modes confined to optical resonators. Section 2 describes cavity-based vibrational optomechanics, and lays the ground for the formalism, basic physics and applications to follow later. Section 3 then introduces OAM-carrying beams. The material presented thus far is then utilized to explain cavity-based torsional and rotational optomechanics in Sections 4 and 5 respectively. Accounting for the more recent interest in cavityless optomechanical systems, we have included some material on this topic in Section 6. The tutorial ends with a Conclusion in Section 7 and Acknowledgments in Section 8.

The format for each section is to first introduce a basic physical configuration. This is done typically, but not in all cases, using work published by our own group, simply because we understand our own work best. Subsequently, reference is made to other works in the field. Although we have tried to be inclusive in making such references, we apologize to all authors whose works are not adequately cited.

2. Vibrational cavity optomechanics

In this section, we will provide a brief review of standard linear vibrational cavity optomechanics [90]; those who are familiar with the material may wish to proceed directly to Section 3. A number of comprehensive reviews of the topic already exist [2, 4, 10, 11], so we will not be aiming to achieve detail or rigor in our presentation. Rather, our discussion will be largely heuristic, focusing on the physics rather than the mathematical details, and aimed mainly at making the ensuing discussion of rotational optomechanics accessible. Although we will be making reference to both classical and quantum regimes for the relevant optomechanical systems, we will largely employ the formalism of second quantization, which makes the notation compact and also reveals the microscopic physics of the system in terms of its fundamental quanta. We begin below by reviewing this formalism for massive particles as well as electromagnetic fields.

2.1. Second quantization for a massive harmonic oscillator

Consider a simple harmonic oscillator of mass m oscillating at frequency ω_m , in one dimension. The corresponding classical mechanical Hamiltonian is given by [90, 86]

$$H = \frac{p^2}{2m} + \frac{1}{2}m\omega_m^2 q^2, \quad (3)$$

where q and p are the oscillator position and momentum, respectively. If we now consider the oscillator to be a quantum object, the two dynamical variables must obey the commutation relation

$$[q, p] = i\hbar, \quad (4)$$

where \hbar is Planck's constant divided by 2π . The dynamical evolution of any quantum mechanical operator O can be found using the Heisenberg equation [86]

$$\dot{O} = \frac{i}{\hbar} [H, O] + \frac{\partial O}{\partial t}, \quad (5)$$

where t is time, the dot denotes a total time derivative, and the last term is nonzero only if the operator carries explicit time-dependence. Using this equation the Heisenberg equations for q and p follow from Eq. (3)

$$\dot{q} = \frac{p}{m}, \quad (6)$$

$$\dot{p} = -m\omega_m^2 q. \quad (7)$$

In real systems, and certainly in optomechanical setups, it is important to account for damping and fluctuations experienced by the oscillator as a result of its coupling to the environment. The procedure for incorporating such effects in a way consistent with quantum mechanics is somewhat complicated and we will not describe it in detail. Fortunately this procedure results in a straightforward prescription called the Quantum Langevin approach [11, 91], which preserves Eq. (6) but modifies Eq. (7), as

$$\dot{q} = \frac{p}{m}, \quad (8)$$

$$\dot{p} = -m\omega_m^2 q - \gamma_m p + \xi, \quad (9)$$

where γ_m is the rate of mechanical damping and ξ is a Brownian stochastic force with zero mean which obeys the correlation function [91]

$$\langle \xi(t)\xi(t') \rangle = \frac{\gamma_m}{\omega_m} \int \frac{d\omega}{2\pi} e^{-i\omega(t-t')} \omega \left[\coth \left(\frac{\hbar\omega}{k_B T} \right) + 1 \right], \quad (10)$$

where k_B is Boltzmann's constant and T is the ambient temperature. Typically we will deal with high temperatures such that $k_B T \gg \hbar\omega_m$. In this limit, the correlation simplifies to

$$\langle \xi(t)\xi(t') \rangle = \frac{2\gamma_m k_B T}{\hbar\omega_m} \delta(t - t'). \quad (11)$$

Working with the quantum mechanical variables q and p is convenient since they allow us to take the classical limit of the theory when required. However, sometimes it is more convenient to use instead a set of variables which describe the system in terms of its basic quanta. Introducing the transformations [90]

$$q = q_0 (b^\dagger + b), \quad p = ip_0 (b^\dagger - b), \quad (12)$$

where

$$q_0 = \sqrt{\frac{\hbar}{2m\omega_m}}, \quad p_0 = \sqrt{\frac{m\hbar\omega_m}{2}}, \quad (13)$$

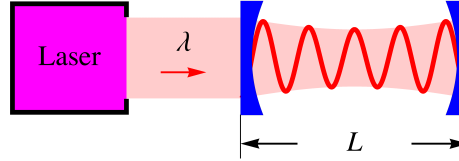


Figure 1. (Color online) Single frequency cavity mode described in Section 2.2. A laser injects light of wavelength λ into a Fabry-Perot cavity made from two highly reflecting mirrors. The cavity length is L .

the Hamiltonian of Eq. (3) can be rewritten as

$$H = \hbar\omega_m b^\dagger b, \quad (14)$$

where we have dropped a constant offset $\hbar\omega_m/2$, which corresponds to the ground state energy of the oscillator, and has no dynamical effect. In this formalism, the operator $b(b^\dagger)$ physically corresponds to the destruction (creation) of one quantum of the oscillator energy, i.e. one phonon. The combination $b^\dagger b$ is called the number operator, as its value denotes the number of quanta carried by the oscillator, with the energy per quantum being $\hbar\omega_m$ as per Eq. (14). From Eqs. (4) and (12), it follows that

$$[b, b^\dagger] = 1. \quad (15)$$

2.2. Cavity quantization of an electromagnetic field mode

We now consider the quantization of a mode of the electromagnetic field, following the approach of Ref. [92]. By a mode we mean an electromagnetic wave of well-defined frequency ω_0 . In order to isolate a single optical mode, it is convenient to use two mirrors facing each other, thus realizing a Fabry-Perot cavity, as shown in Fig.1. The classical electromagnetic Hamiltonian, which combines the electric and magnetic contributions, is given by [92]

$$H_0 = \frac{1}{2} \int dV \left[\epsilon_0 E^2 + \frac{B^2}{\mu_0} \right], \quad (16)$$

where E and B are the electric and magnetic fields, respectively, and the integration is over the cavity volume. As a useful idealization, the two mirrors, which are a length L apart, are taken to be perfectly reflecting. This assumption will be relaxed later. The quantized electric and magnetic fields which satisfy the appropriate boundary conditions are

$$E_x(z, t) = E_0 (a^\dagger + a) \sin kz, \quad (17)$$

$$B_y(z, t) = iB_0 (a^\dagger - a) \cos kz, \quad (18)$$

where

$$E_0 = \left(\frac{\hbar\omega_0}{\epsilon_0 V} \right)^{1/2}, \quad (19)$$

$$B_0 = \frac{\mu_0}{k} \left(\frac{\epsilon_0 \hbar \omega_0^3}{V} \right)^{1/2}, \quad (20)$$

are sometimes referred to as the electric and magnetic fields “per photon”. In Eqs. (17) and (18), the wavenumber

$$k = \frac{\omega_0}{c}, \quad (21)$$

where c is the speed of light, and the optical field frequency is given by

$$\omega_0 = \frac{n\pi c}{L}, \quad n = 1, 2, 3, \dots, \quad (22)$$

which follows from the physical requirement that the length of the cavity has to be an integer number of half wavelengths to support the electromagnetic mode. Using the fields of Eqs. (17) and Eqs. (18) in Eq. (16) yields the harmonic oscillator Hamiltonian

$$H_0 = \hbar\omega_0 a^\dagger a. \quad (23)$$

The variables a and a^\dagger correspond to destruction and creation operators for the photons confined to the cavity, and

$$[a, a^\dagger] = 1. \quad (24)$$

Realistically, of course, the Fabry-Perot mirrors are not perfectly reflecting. In fact, some degree of transmission is required so photons can be injected into the cavity, typically by a laser. To account for this driving, the Hamiltonian of Eq. (23) is modified to [11]

$$H_0 = \hbar\omega_0 a^\dagger a + i\hbar F (a^\dagger e^{-i\omega_l t} - a e^{i\omega_l t}), \quad (25)$$

where ω_l is the frequency of the driving laser, F is related to the input laser power P by

$$F = \sqrt{\frac{P\gamma_0}{\hbar\omega_0}}, \quad (26)$$

and γ_0 is the rate at which photons leak from the cavity.

The dynamical evolution of a can be obtained from Eq. (5) (we presently ignore the effects of γ_0 on this equation, but see Eq. (31) below)

$$\dot{a} = -i\omega_0 a + F e^{-i\omega_l t}, \quad (27)$$

which can be transformed using the substitution (which corresponds to entering the frame rotating at the frequency of the input laser)

$$a \rightarrow a e^{i\omega_l t}, \quad (28)$$

to the equation

$$\dot{a} = -i\Delta_0 a + F, \quad (29)$$

where

$$\Delta_0 = \omega_0 - \omega_l, \quad (30)$$

is the detuning of the laser from the cavity. The presence of the cavity mirror transmissivity also introduces dissipation and noise into the cavity. The effect of these

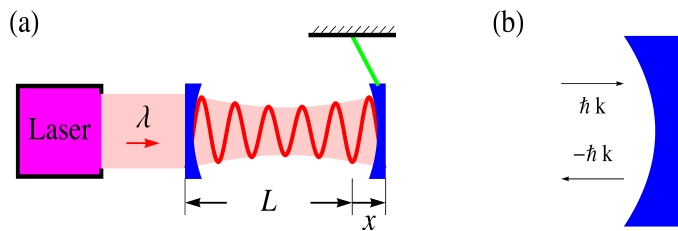


Figure 2. (Color online) (a) An optomechanical cavity. The arrangement is the same as in Fig. 1, but with one of the mirrors mounted as a harmonically oscillating pendulum with amplitude x measured from its equilibrium position. (b) Reversal of the photon momentum upon reflection from a perfectly reflecting mirror.

disturbances on the optical mode can be accommodated using the Quantum Langevin approach and changes the time evolution of Eq. (29) to [11]

$$\dot{a} = -i\Delta_0 a - \frac{\gamma_0}{2} a + \sqrt{\gamma_0} a_{\text{in}} + F, \quad (31)$$

where a_{in} is the electromagnetic noise that comes in through the transmissive mirror, and has zero mean and the correlator [91]

$$\langle a_{\text{in}}(t) a_{\text{in}}^\dagger(t') \rangle = \delta(t - t'). \quad (32)$$

at optical frequencies. The presence of the cavity decay γ_0 introduces a nonzero width to the frequency ω_0 of the electromagnetic field. With this inclusion of photon loss from the cavity, the optical field is referred to as a *quasi-mode*. Note that according to Eq. (31) the field variables a and a^\dagger each decay at the rate $\gamma_0/2$, while the oscillator energy decays at γ_0 . In the classical limit, the operator a can be replaced by the complex-valued dynamical variable $\alpha(t)$, which corresponds to the amplitude of the classical electromagnetic field [92]. In this limit, the number of photons in the cavity is $|\alpha(t)|^2$.

2.3. Optomechanical cavity

We now consider a Fabry-Perot cavity where one mirror is fixed but the other is allowed to oscillate harmonically along the cavity axis. This can be accomplished by suspending it like a pendulum, as in Fig. 2(a), or by mounting it on a spring, for instance. We will derive the Hamiltonian for this system using heuristic semiclassical arguments [90]; a rigorous quantum mechanical description can be found in [93]. If the mechanical oscillation frequency ω_m is much smaller than the spacing between two neighboring modes of the cavity, then we can consider a single optical mode, since photon scattering into neighboring modes is then negligible. Let us assume first that the two mirrors are both perfectly reflecting, and consider the reflection of a single photon, as shown in Fig. 2(b). The photon momentum before reflection is $\hbar k$ and after reflection is $-\hbar k$. The net change of momentum of the photon is therefore $2\hbar k$. The reflected photon

returns after being reflected from the stationary mirror, after a time $2L/c$. The change of momentum per unit time, i.e. the force exerted by each photon is

$$\hbar g = \frac{2\hbar k}{2L/c}, \quad (33)$$

from which the optomechanical coupling constant may be written as

$$g = \frac{ck}{L}, \quad (34)$$

or using Eq. (22) as

$$g = \frac{\omega_0}{L}. \quad (35)$$

The total force due to all the photons present in the cavity is therefore $\hbar g a^\dagger a$. The work extracted by the optical field in moving the mechanical oscillator from L to $L + q$ yields the energy of optomechanical interaction

$$H_{\text{int}} = -\hbar g a^\dagger a q, \quad (36)$$

where all dynamical variables are quantum mechanical. The full optomechanical Hamiltonian then combines Eqs. (23), (25), and (36)

$$H_{OM} = \frac{p^2}{2m} + \frac{1}{2}m\omega_m^2 q^2 + \hbar\omega_0 a^\dagger a - \hbar g a^\dagger a q + i\hbar F (a^\dagger e^{-i\omega_l t} - a e^{i\omega_l t}). \quad (37)$$

In order to remove the explicit time-dependence, a transformation

$$U = e^{i\omega_l a^\dagger a t}, \quad (38)$$

into the frame rotating with the driving laser may be made, yielding,

$$H'_{OM} = U H_{OM} U^\dagger - i\hbar U \frac{\partial U^\dagger}{\partial t}, \quad (39)$$

or explicitly,

$$H'_{OM} = \frac{p^2}{2m} + \frac{1}{2}m\omega_m^2 q^2 + \hbar\Delta_0 a^\dagger a - \hbar g a^\dagger a q + i\hbar F (a^\dagger - a). \quad (40)$$

Sometimes it is convenient to use the variables of Eq. (12),

$$H'_{OM} = \hbar\Delta_0 a^\dagger a + \hbar\omega_m b^\dagger b - \hbar g' a^\dagger a (b^\dagger + b) + i\hbar F (a^\dagger - a), \quad (41)$$

where

$$g' = gq_0. \quad (42)$$

Accounting for noise and dissipation, the Quantum Langevin Equations for the optomechanical cavity are

$$\dot{q} = \frac{p}{m}, \quad (43)$$

$$\dot{p} = -m\omega_m^2 q - \gamma_m p + \xi, \quad (44)$$

$$\dot{a} = -\left(i\Delta_0 + \frac{\gamma_0}{2}\right) a + ig' a q + F + \sqrt{\gamma_0} a_{\text{in}}. \quad (45)$$

2.4. Optomechanical sensing and cooling of mechanical motion

While the optomechanical cavity described above is associated with several physical phenomena, we will briefly discuss only two below: displacement sensing and cooling of mechanical motion. This abbreviated discussion will be sufficient for motivating the introduction of rotational optomechanics below. For readers interested in other effects, such as bistability, squeezing, etc., we recommend several available reviews [2, 3, 4, 10, 11].

Displacement sensing using optomechanical platforms is an application that relies on the fact that a cavity photon picks up a phase that depends on the distance it travels, and hence on the displacement of the mechanical oscillator in Fig. 2. Mathematically, we can see from Eq. (45) that the time evolution of the optical mode a depends on the oscillator displacement q . To investigate further, let us assume the so-called ‘bad cavity’ limit, where γ_0 is large and the photons leave the cavity so quickly that the optical mode can rapidly adjust to instantaneous position of the oscillator. In this regime, we can adiabatically eliminate the cavity mode, by setting \dot{a} in Eq. (45) to zero. This procedure yields

$$a = \frac{F}{\frac{\gamma_0}{2} + i(\Delta_0 + g'q)}, \quad (46)$$

which shows the dependence of a on q . Rewriting in polar form, and assuming $\Delta_0 = 0$ for simplicity,

$$a(\Delta_0 = 0) = \frac{F}{\left[\left(\frac{\gamma_0}{2}\right)^2 + (g'q)^2\right]^{1/2}} e^{i \tan^{-1}\left(-\frac{g'q}{\gamma_0/2}\right)}, \quad (47)$$

which shows that the oscillator position information is contained in both the amplitude as well as the phase of the cavity mode. In particular, the phase becomes more sensitive to q if g'/γ_0 is large, i.e. for stronger optomechanical coupling and low-loss cavities (although we are in the high loss limit). A more detailed analysis shows that in the ‘good cavity’ limit (γ_0 small), the displacement sensitivity of the device improves with the cavity finesse [11]. This principle is the basis of interferometers such as LIGO which seek to transduce weak gravitational waves into detectable mechanical displacements [7].

Optical cooling of the mechanical motion is another application of the optomechanical cavity [11]. Neglecting dissipation, noise and driving for simplicity, Eq. (41) reads

$$H'_{OM} = \hbar\Delta_0 a^\dagger a + \hbar\omega_m b^\dagger b - \hbar g' a^\dagger a (b^\dagger + b). \quad (48)$$

The interaction term proportional to $a^\dagger ab$ corresponds to cooling of the mechanical motion, since it describes a process in which a photon (a) and a phonon (b) are annihilated while a second photon (a^\dagger) is created. Since energy has to be conserved during this process, the second photon must have higher energy than the first, by exactly $\hbar\omega_m$, the phonon energy. This is allowed because the photons belong to a quasi-mode

with nonzero linewidth, and need not both have exactly the same frequency. The key point is that the annihilation of a phonon cools the mechanical motion of the oscillator. Using similar arguments, it can be shown that the interaction term proportional to $a^\dagger ab^\dagger$ corresponds to oscillator heating. A detailed treatment indicates that by tuning the driving laser to below the cavity resonance ($\Delta_0 > 0$) allows the cooling to dominate over the heating; such a scheme has been used for laser cooling a mesoscopic mechanical oscillator to its quantum ground state [14].

3. Optical beams carrying angular momentum

In this section, we will provide a brief introduction to optical beams carrying angular momentum [94]. We will assume the reader is familiar with the fact that a photon can have spin angular momentum $\pm\hbar$, corresponding classically to circularly polarized radiation. This is one way in which optical beams can carry angular momentum. Another way is by encoding the appropriate structure in the beam phase [32, 33, 34, 35, 36, 37, 38, 40, 41, 42]. Each photon in the beam can then be thought of as carrying an OAM which can take unlimited values in principle, and quite high values in practice. Although a clear separation of spin and orbital angular momentum degrees of freedom is generally a subtle matter [32, 34], in this article we will operate under conditions where the requirements for effecting this separation are fulfilled. Specifically, we will work in the paraxial regime of beam propagation, where the separation is valid. Below we will introduce OAM-carrying beams by discussing a specific method for their generation. Based on this discussion we will consider some general properties of such beams, which come in several families [42]. Subsequently, we will consider a particular family, namely the Laguerre-Gaussian modes, for a more detailed exposition.

3.1. Generation of OAM-carrying beams

There are several ways of generating beams carrying OAM, such as using lasers, lenses, holograms, spatial light modulators and spiral phase plates [36]. We will consider the relevant case of a spiral phase plate, shown in Fig. 3(b). To understand what such a phase plate does to an optical beam, we first consider the simpler case of the same beam passing through a uniform slab of thickness L , as shown in Fig. 3(a). If the beam incident on the slab is modeled as a plane wave of amplitude E_0 , it will pick up a phase on transmission, leading to an output field $E'_0 e^{ikL}$, where E'_0 is the amplitude of the transmitted radiation, k is the wavevector of the optical beam, and $\hbar k$ is the linear momentum per photon. The optical phase acquired by the beam therefore depends on the thickness L of the slab.

When the same beam passes through the spiral phase plate, which has a uniform azimuthal gradient in its thickness, it picks up a phase which depends on the angle ϕ about the light propagation direction,

$$E_0 \rightarrow E'_0 e^{il\phi}, \quad (49)$$

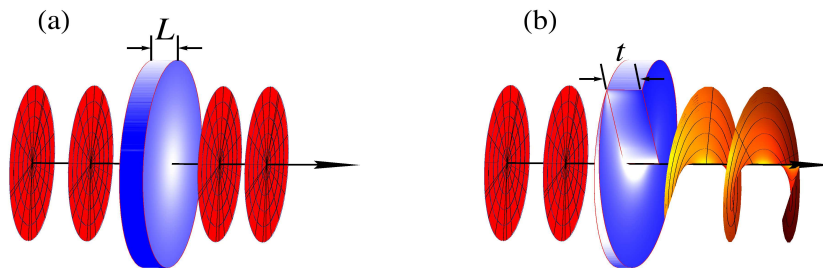


Figure 3. (Color online) (a) Transmission of the wavefronts of a plane wave through a uniform slab of thickness L (b) Transmission of the wavefronts of a plane wave through a spiral phase plate of step height t . The transmitted wavefronts in this case are helicoidal. Adapted with permission from [42].

where

$$l = \frac{t}{\lambda}, \quad (50)$$

t is the step height of the phase plate, and λ the optical wavelength. Analogous to the linear phase factor discussed above, where $\hbar k$ is the linear momentum, $\hbar l$ can be identified as the orbital angular momentum carried by each photon in the transmitted beam. This identification can be verified by rigorously calculating the angular momentum carried by the electromagnetic fields of the beam [46]. By arranging for the plate thickness to be an integer multiple of the optical wavelength, we will restrict ourselves to integer values of l in Eq. (50). If l is not an integer, the transmitted beam consists of an infinite superposition of integer- l' waves, whose average OAM is then the non-integer value given by Eq. (50).

Although we have considered transmission through the spiral phase plate in our example above, reflected photons pick up orbital angular momentum as well. In both cases the angular momentum is supplied by the spiral phase plate. Usually the plate is clamped to an optical table and serves as a virtually infinite source or sink of angular momentum. Lastly, we point out that the azimuthal phase factor $e^{il\phi}$ in the field transmitted by the spiral phase plate is well-defined everywhere except on the z axis, as ϕ is multiply defined on that line. In a consistent physical picture of the field, the amplitude vanishes on the z -axis, and the beam resultantly carries a singularity, namely a vortex. The intensity profile of the beam therefore presents a node at the core of the vortex, i.e. on the z axis, see Fig. 4 below. The OAM l , which quantifies the beam vorticity, is sometimes referred to as the ‘topological charge’ of the optical beam.

We have presented an idealized description thus far, using a plane wave, which has infinite transverse extent. In practice, the beam has a transverse profile which decreases

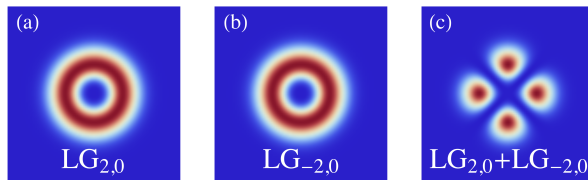


Figure 4. (Color online) (a) Intensity pattern for an $l = 2, p = 0$ Laguerre-Gaussian beam (b) Intensity pattern for an $l = -2, p = 0$ Laguerre-Gaussian beam (c) Intensity pattern for a superposition of $l = 2, p = 0$ and $l = -2, p = 0$ Laguerre-Gaussian beams.

in intensity away from the propagation axis. We now move on to the discussion of such modes.

3.2. Laguerre-Gaussian modes

An appropriate expression for an OAM-carrying field is

$$E(\mathbf{r}) = u(\mathbf{r}) e^{il\phi}, \quad (51)$$

which accounts for the transverse coordinate dependence of the field. Fields of this type form solutions to the paraxial wave equation in free space and are therefore bonafide modes of the electromagnetic field in that approximation [37]. There are several families of beams that carry OAM, corresponding to different forms for $u(\mathbf{r})$, including Bessel, Mathieu, and Hypergeometric-Gaussian modes [42]. We consider the Laguerre-Gaussian fields for which

$$E(\mathbf{r}) = u_{lp}(\mathbf{r}) e^{il\phi}, \quad (52)$$

and the normalized mode function is given by [37]

$$u_{lp}(\mathbf{r}) = \frac{C_{lp}}{\sqrt{w(z)}} \left[\frac{\rho\sqrt{2}}{w(z)} \right]^{|l|} e^{-\frac{\rho^2}{w^2(z)}} L_p^{|l|} \left[\frac{2\rho^2}{w^2(z)} \right] e^{\frac{-ik\rho^2 z}{2(z_R+z^2)}} e^{il\phi} e^{i(2p+|l|+1)\tan^{-1}\left(\frac{z}{z_R}\right)}, \quad (53)$$

where the normalization

$$C_{lp} = \sqrt{\frac{2^{|l|+1}p!}{\pi(p+|l|)}}, \quad (54)$$

the index l corresponds to the number of azimuthal nodes, the index p determines the number of radial nodes [95], $w(z)$ is the beam waist, $L_p^{|l|}$ is the associated Laguerre polynomial, and $z_R = \pi w^2(0)/\lambda$ is the Rayleigh range, λ being the optical wavelength. In Eq. (53), l can be either a positive or negative integer, while p can only assume positive integer values.

The intensity profile of a Laguerre-Gaussian mode with $l \neq 0$ has a node at the center, and appears shaped as an annulus, see Fig. 4(a) for $l = 2$. The interference pattern between two $LG_{\pm l}$ beams consists of $2l$ lobes arranged in a circle, see Fig. 4(c) for the case where $l = 2$. With this brief introduction to OAM-carrying beams, we are now ready to combine mechanical motion with photonic angular momentum.

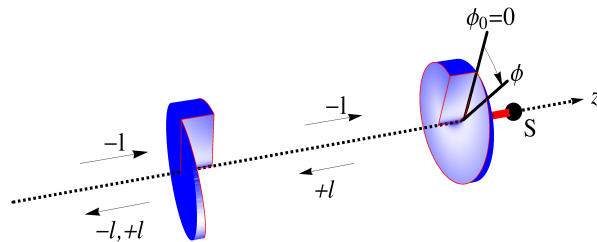


Figure 5. (Color online) A picture of the spiral resonator discussed in Section 4.1. Adapted with permission from [96].

4. Torsional cavity optomechanics

In this section, we will consider some optomechanical platforms that couple photonic angular momentum to mechanical torsional motion. We will first introduce a straightforward analog of the linear optomechanical cavity presented in Section 2.3, and then consider a variation on the same theme.

4.1. Spiral Resonator

We begin with a torsional analog to the standard linear vibrational optomechanical cavity of Section 2.3 [96], as shown in Fig. 5. In this analogy, the spherical mirrors used in a Fabry-Perot are replaced by spiral phase plates described in Section 3.1. One of the plates is fixed in place, while the other oscillates harmonically about the cavity axis, thus executing torsional motion. The angular displacement of the moving plate is measured by the angle ϕ . A beam with OAM $l\hbar$ is incident on the cavity. The spiral phase plates reverse the linear momentum as well as the OAM of the cavity photons upon reflection. This reversal of OAM can be arranged by selecting the step heights and handedness on the spiral plates so that one of them adds, and the other subtracts, the same OAM from the cavity photons, as shown in Fig. 5. The optomechanical coupling can be derived analogously to Section 2.3 if we assume that the two spiral phase plates are perfectly reflecting. In this case, the moving plate reverses the photonic OAM from $l\hbar$ to $-l\hbar$ upon reflection, resulting in a momentum change of $2l\hbar$ per photon. This happens once every cavity round trip time $2L/c$, if the cavity length is L . The change of angular momentum per unit time, i.e. the torque exerted by each photon is given by

$$\hbar g_\phi = \frac{2\hbar l}{2L/c}, \quad (55)$$

which may be compared to Eq. (35) and from which the *optotorsional* coupling constant, may be obtained as

$$g_\phi = \frac{cl}{L}, \quad (56)$$

which is analogous to Eq. (34). The total torque due to all the photons present in the cavity is $\hbar g_\phi a^\dagger a$. The work extracted from the torsional oscillator in deflecting it by an angle ϕ yields the energy of optomechanical interaction

$$H_{\text{int}}^\phi = -\hbar g_\phi a^\dagger a \phi, \quad (57)$$

The entire optomechanical Hamiltonian may now be assembled in analogy to Eq. (40)

$$H_{OM}^\phi = \frac{L_z^2}{2I} + \frac{1}{2}I\omega_\phi^2\phi^2 + \hbar\Delta_0 a^\dagger a - \hbar g_\phi a^\dagger a \phi + i\hbar F (a^\dagger - a), \quad (58)$$

where L_z is the angular momentum of the oscillating spiral phase plate about the cavity axis, I is its moment of inertia, and ω_ϕ is the frequency of torsional oscillation. The first two terms describe the torsional energy of oscillation, the third term the optical mode energy, the fourth term the optomechanical interaction, and the fifth term the effect of external driving on the cavity. If the moving spiral phase plate has mass M and radius R , we may treat it as a disk and evaluate the moment of inertia

$$I = \frac{MR^2}{2}, \quad (59)$$

about an axis passing through its center. In Eq. (58), all dynamical variables are quantum mechanical. Specifically, the torsional variables obey the commutation relation

$$[L_z, \phi] = -i\hbar. \quad (60)$$

Since Eq. (58) has the same form as Eq. (40), we may expect to implement the same optomechanical physics on this new platform, i.e. detection of torsional displacements as well as cooling of torsional motion should be possible. Interestingly, the optotorsional coupling in (56) depends on l , which may be adjusted by the experimentalist. In recent experiments, upto $l = 300$ has been used [97].

Unlike the standard Fabry-Perot, which has been investigated for more than a century, the spiral phase plate resonator appeared in the theoretical literature only once (without the mechanical degree of freedom) [98] before the optomechanical version was proposed. Therefore, much fundamental information about the spiral resonator remains to be discovered. As a first step in this direction, our group has recently analyzed the ray optics of this resonator [99]; related work has also recently been carried out for low finesse spiral etalons [100]. No experimental realization of the spiral phase resonator seems to exist, possibly due to the low reflectivity ($\leq 95\%$) and high diffractive losses presented by currently available spiral phase plates. These limitations preclude the implementation of efficient displacement sensing or torsional cooling, both of which require high-finesse cavities. Interestingly, a design equivalent to a spiral phase resonator (but without any mechanical degrees of freedom) has been implemented in a situation where the mirror losses are offset by the presence of a gain medium - i.e. in a laser [101].

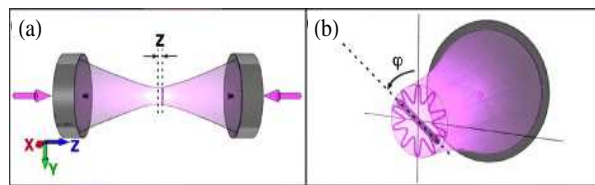


Figure 6. (Color online) The system discussed in Section 4.2. (a) shows the trapping configuration along the cavity axis (b) shows the angular optical lattice in which the rod is trapped and executes torsional motion about the cavity axis. Adapted with permission from [102].

4.2. Nanorods and Windmills

In this section we will consider the proposal of Romero-Isart et al. [102] for coupling a rod to OAM-carrying cavity modes, and its subsequent generalization to nano-windmills [103]. These proposals rely on the ability of light to optically trap dielectric particles at the intensity maxima of an optical beam. The trapping may be understood intuitively if the dielectric particle is smaller than an optical wavelength and thus may be assumed to behave as a point dipole. If the dipole moment is \vec{d} , the energy of interaction with an optical beam of electric field \vec{E} is

$$H_t = -\vec{d} \cdot \vec{E}. \quad (61)$$

If the particle is a neutral but linearly polarizable dielectric, with polarizability α , then the dipole moment is an induced one, and is given by

$$\vec{d} = \alpha \vec{E}. \quad (62)$$

Combining Eqs. (61) and (62), we obtain

$$H_t = -\alpha |\vec{E}|^2. \quad (63)$$

Now since $|\vec{E}|^2 = 2I_0/c\epsilon_0$ where I_0 is the light intensity, clearly H_t is a minimum when the particle is located at an intensity maximum of the beam. At such maxima, in fact, the force from the optical beam can levitate the particle in space against the effect of gravity. In practice, it is quite common to use the focus of a Gaussian beam as an optical trap for the particle [76]. To lowest order in the particle displacement, such a trap provides harmonic confinement in all three directions in space.

In their proposal, Romero-Isart suggest trapping a nanorod with multiple Laguerre-Gaussian cavity modes, in such a manner that the rod executes torsional oscillations about the cavity axis, see Fig. 6. The trapping field is considered to be an experimentally changeable parameter and does not possess dynamics of its own. An additional Laguerre-Gaussian mode with $p = 0$ is introduced to detect and cool the torsional oscillations. The corresponding Hamiltonian is essentially of the same form as in Eq. (58), and therefore we do not repeat its full derivation here. We only note that the optomechanical coupling

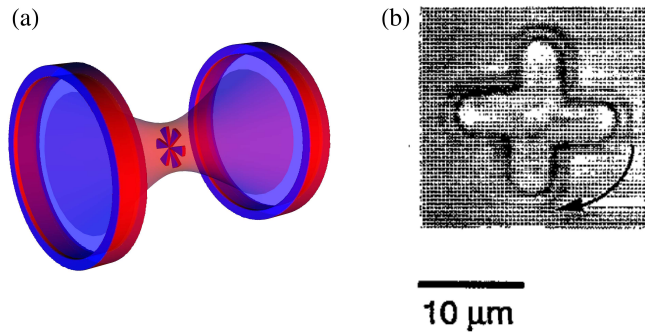


Figure 7. (Color online) (a) A nanowindmill levitated inside an optical cavity. Adapted with permission from [103] (b) A photomicrograph of a microfabricated windmill. Reproduced with permission from [105].

in the case of the rod was calculated using the Bethe-Schwinger perturbation theory formula [104]

$$\frac{\omega_c(\phi)}{\omega_c(\phi_0)} \simeq 1 - \frac{\int_V (\epsilon - 1) |u_{l0}(\mathbf{r})|^2 d\mathbf{r}}{2 \int_{V'} |u_{l0}(\mathbf{r})|^2 d\mathbf{r}}, \quad (64)$$

which accounts for the variation of the cavity resonance $\omega_c(\phi)$ due to the change in the angular position of the rod ϕ away from its equilibrium value ϕ_0 and where ϵ and V are the dielectric constant and volume, respectively, of the windmill, and V' is the volume of the optical cavity. The optomechanical coupling can then be found as

$$g_{l,0} = \sqrt{\frac{\hbar}{I\omega_\phi} \frac{\partial \omega_c(\phi)}{\partial \phi|_{\phi_0}}}, \quad (65)$$

from Eq. (64). The Bethe-Schwinger formula is applicable when the dimensions of the rod are small enough that its presence in the cavity shifts the optical resonance only by a small amount. Interestingly, the authors point out that a suitable nanorod could be the Tobacco Mosaic Virus, thus opening up a way to observe quantum effects in living organisms.

The work of Romero-Isart et al., has been generalized further by considering, instead of a single rod, a windmill-shaped dielectric, which may be thought of as a collection of rods, see Fig. 7(a) [103]. The advantage of a windmill shape is that it provides larger overlap with the cavity OAM modes than a single rod, and hence higher optomechanical coupling. We note that micromachined windmills are available in the laboratory, and have been held and rotated in optical tweezers using radiation pressure from optical beams [105], see Fig. 7(b). While Romero-Isart considered only $p = 0$ beams [see Eq. (53)], it was later found that using modes with nonzero p yields better optomechanical coupling, since such modes match the shape of the windmill better [103].

A recent experimental development along these lines was the demonstration of the transit of rotating nanorods through an optical cavity excited by a Gaussian optical beam [106]. More sophisticated theoretical proposals also exist, incorporating multiple

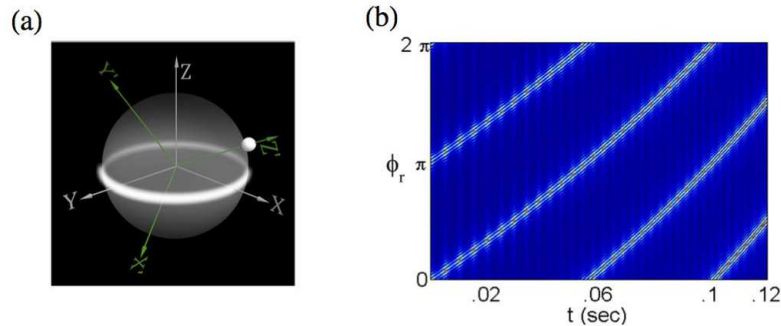


Figure 8. (Color online) (a) The system described in Section 5.1. The large circle denotes a microsphere, the bright band along the equator is a whispering gallery mode which confines the optical field, and the small circle is a nanoparticle trapped in orbit around the sphere (b) Surface field intensity at the microsphere equator as a function of time. Reproduced with permission from [109].

nanodumbbells into an optical cavity and predicting optically induced ordering and nematic transitions analogous to those observed in liquid crystals [107]. Torsional optomechanics realized by coupling wave guide deformations with circularly polarized photons has also been proposed [108]. Thus far we have considered the coupling of optical angular momentum to mechanical torsional motion. We now proceed to examine the coupling of optical angular momentum with free mechanical rotation.

5. Rotational cavity optomechanics

In this section we introduce the coupling of optical angular momentum with unhindered mechanical rotation. First we consider a particle rotating in the evanescent field of an optical resonator, and then a configuration in which the particle experiences the intracavity field.

5.1. Evanescently trapped nanoparticle

In this section, we consider a subwavelength dielectric particle captured in orbital motion around a spherical whispering gallery mode resonator, as analyzed by Rubin et al. [109, 110], and shown in Fig. 8 (a). To our knowledge, this was the first configuration in which fully rotational cavity optomechanics was studied [111]. The resonator itself is a dielectric microsphere. The optical mode is confined by total internal reflection near the surface of the resonator; the authors specifically consider whispering gallery modes that are localized near the resonator equator, as in Fig. 8. Some of the light escapes from the spherical resonator in the form of an evanescent field. It is this light that is responsible for trapping the subwavelength dielectric particle ‘and driving its motion. The optomechanical coupling in this case is somewhat complicated and will not be derived here. The complications arise because the particle stays quite close to

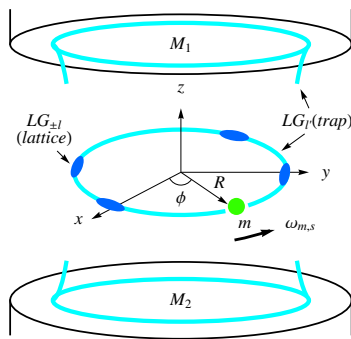


Figure 9. (Color online) The system referred to in Section 5.2. A nanoparticle of mass m rotates around an optical ring potential and is probed by an angular optical lattice inside a cavity. Reproduced with permission from [112].

the dielectric sphere and therefore modifies the charge distribution on the resonator, effects which are negligible in the optomechanical systems described thus far.

The resulting particle dynamics are also quite involved. The radial, polar and azimuthal motions of the particle are driven by the radiation field, and are coupled to each other. In particular, the orbital rotation of the particle about the spherical resonator is driven by the optical torque, which turns out to be nonconservative. However, as in standard optomechanics, the particle motion acts back on the field and therefore can be deciphered by monitoring, for example, the field intensity at the resonator surface. Figure 8(b) shows the surface field intensity along the resonator equator. The intensity variations along the horizontal axis represent radial particle oscillations, and from their non-uniform spacing the angular azimuthal acceleration of the particle can be found. Similarly, the intensity variations along the vertical axis correspond to polar oscillations. While this configuration displays many interesting features, the role played by electromagnetic angular momentum is somewhat limited. Assuming dipolar scattering of photons, the authors show that the nanoparticle couples only to three optical angular momenta, namely 0 and $\pm h$.

5.2. Nanoparticle rotating inside a cavity

In this section we will analyze a rotating nanoparticle located *inside* an optical cavity, as shown in Fig. 9 [112]. Unlike in the configuration of Section 5.1, the usual light-matter coupling applies. This is because the rotating particle is far away from the resonator boundaries. This configuration is the free rotational analog of the linear optomechanical system of Section 2.3, and we will examine it in some detail. Our exposition below will be aimed at establishing the possibility of accurate rotation sensing, i.e. implementing velocimetry of the particle, using a cavity. We will restrict ourselves to a classical analysis. A quantum analysis of rotation is expected to be more subtle [113],

The optical resonator in this case is a Fabry-Perot, with both mirrors fixed in place. The cavity is excited by a trap beam, which is a Laguerre-Gaussian mode with OAM

$l_t = 2$. This mode presents an intensity maximum on a ring [see Fig. 9 and also Fig. 4(b)] of radius

$$R = w_0 \left(\frac{|l_t|}{2} \right)^{1/2}, \quad (66)$$

at the center of the cavity. A dielectric particle of diameter smaller than the optical wavelength is trapped on this ring via the optical gradient force, see Eqs (63). We consider this particle to be rotating on this ring at a uniform angular velocity $\omega_{m,s}$ set by the balance of an external torque and the damping produced by the background gas particles as realized experimentally [114]. We assume conditions where the coupling to radial and polar motion are negligible, i.e. tight confinement on the ring, and do not consider these degrees of freedom any further. The trap mode is treated as a parametric quantity, without any associated dynamics.

An additional optical field, a superposition of two degenerate counter-rotating Laguerre-Gaussian modes with OAM $+l$ and $-l$ respectively, is introduced to probe the rotational motion of the nanoparticle. Near the trapping ring, the modes set up an optical lattice with $2l$ maxima, described by the function

$$|u_{l,0}|^2 = \frac{1}{|l|!} \left(\frac{R\sqrt{2}}{w_0} \right)^{|l|} e^{-\frac{2R^2}{w_0^2}} \cos^2(k_p z) \cos^2(\phi), \quad (67)$$

where k_p is the probe wave-vector. Figure 4(c) and Fig. 9 show the lattice for $l = 2$. Since the particle dimensions are smaller than the cavity length L and the optical wavelength λ , Eq. (64) can be used to find the optorotational coupling $g(l)$, using Eq. (67) as the input. This yields

$$\omega_c(\phi) = \omega_c - g(l) \cos^2 l\phi, \quad (68)$$

with

$$g(l) = (\epsilon_r - 1) \frac{2^{\frac{l+3}{2}}}{\Gamma\left(\frac{l+1}{2}\right)} \left(\frac{R}{w_0} \right)^l \frac{V}{\pi w_0^2 L} e^{-\frac{2R^2}{w_0^2}}, \quad (69)$$

where ϵ_r is the relative dielectric constant of the nanoparticle and Γ is a Gamma function.

The dynamics of the optical probe field can be described using the variable $a(t)$ such that $|a(t)|^2$ is the number of probe photons inside the cavity at any time t , see the very end of Section 2.2. Choosing the cavity axis as the z direction, the angular momentum of the particle is L_z . To describe the rotational coordinate of the particle we use the periodic variable

$$U_l = e^{2il\phi}, \quad (70)$$

where ϕ is the instantaneous angular displacement of the particle, see Fig. 9.

The coupled equations of motion in the frame of the laser driving the cavity with the LG_{\pm} fields can be written in analogy to Eqs. (43)-(45)

$$\dot{U}_l = \frac{i2lU_l L_z}{I}, \quad (71)$$

$$\dot{L}_z = -\gamma_m L_z - 2il\hbar g(l) (U_l - U_l^*) |a(t)|^2 + \tau + \tau_{in}. \quad (72)$$

$$\dot{a} = \left\{ i \left[\Delta' - \frac{g(l)}{2} (U_l + U_l^*) \right] - \frac{\gamma_0}{2} \right\} a + \sqrt{\gamma} a_{in}, \quad (73)$$

where

$$\Delta' = \Delta - \frac{g(l)}{2}, \quad (74)$$

$\Delta = \omega_d - \omega_c$ being the detuning between the $LG_{\pm l}$ driving laser at frequency ω_d and ω_c , γ_0 is the cavity loss rate, $I = mR^2$ is the dielectric particle's moment of inertia about the axis of rotation and $a_{in} = \sqrt{P_{in}/\hbar\omega_c}$, where P_{in} is the input probe power. Classical laser noise and the thermal contribution to the radiation mode have been assumed to be negligible. The rotor mechanical damping is γ_m , and τ_{in} is a Langevin torque with zero mean and the two-time fluctuation correlation (analogous to Eq. 11)

$$\langle \delta\tau_{in}(t)\delta\tau_{in}(t') \rangle = 2I\gamma_m k_B T \delta(t - t'), \quad (75)$$

signifying white noise and responsible for Brownian motion. Generally, we will assume that the externally applied torque is larger than the torque due to the optical lattice, i.e. $\tau > 2il\hbar g(l) (U_l - U_l^*) |a(t)|^2$.

Comparing Eq. (73) to Eq. (45) shows that the phase of the optical field is sensitive to the $(U_l + U_l^*)/2 = \cos 2l\phi$ quadrature of the mechanical rotation, and that this sensitivity improves linearly with the cavity finesse, and may therefore be used to accurately detect the particle rotation. We elaborate on this procedure below. The steady-state of the system can be found readily by equating the time derivatives in Eqs. (73)-(72) to zero,

$$\omega_{m,s} = \frac{L_{z,s}}{I} = \frac{\tau}{I\gamma_m}, \quad (76)$$

$$U_{l,s} = 0, \quad (77)$$

$$a_s = \frac{\sqrt{\gamma} a_{in}}{\left[\Delta'^2 + \left(\frac{\gamma_0}{2} \right)^2 \right]^{1/2}}. \quad (78)$$

We note from Equation (76) that the torque due to the probe lattice makes no contribution, on average, to the rotation rate $\omega_{m,s}$. We can examine the linear response of the system (i.e. the response of the system to small changes away from the steady state) by considering each variable as the sum of a mean value and a small fluctuation, e.g.

$$a = a_s + \delta a. \quad (79)$$

For low probe powers, we find

$$\begin{aligned} \dot{\delta a} &= -i \frac{g(l)}{2} a_s (\delta U_l + \delta U_l^*) + \left(i\Delta' - \frac{\gamma}{2} \right) \delta a, \\ \delta \dot{U}_l &= \frac{i2l}{I} L_{z,s} \delta U_l, \\ \delta \dot{L}_z &= -\gamma_m \delta L_z + 2il\hbar g(l) |a_s|^2 (\delta U_l - \delta U_l^*) + \delta \tau_{in}. \end{aligned} \quad (80)$$

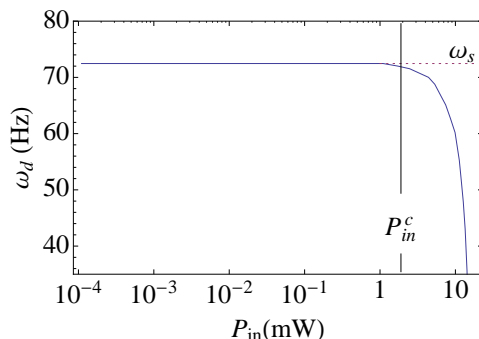


Figure 10. (Color online) The optically detected mechanical rotation frequency ω_d as a function of probe lattice power P_{in} in the setup of Fig. (9). The detected frequency accurately mirrors the rate ω_s [Eq. (84)] in the regime of linear response, i.e. for probe power less than P_{in}^c , but is affected for higher powers, degrading the accuracy of the measurement. Adapted with permission from [112].

Solving this set of equations given the initial conditions $\delta a(0)$, $\delta U_l(0)$ and $\delta L_z(0)$, we find on resonance ($\Delta' = 0$), and ignoring cavity losses ($\gamma_0 = 0$), that the Fourier transform of $\delta a(t)$ is

$$\delta a(\omega) = A\delta(\omega) + B^*\delta(\omega - \omega_s) - B\delta(\omega + \omega_s), \quad (81)$$

where

$$A = \sqrt{2\pi}\delta a(0) + B - B^*, \quad (82)$$

$$B = \frac{\sqrt{2\pi}a_s g(l)\delta U_l(0)}{\omega_{m,s}}, \quad (83)$$

and

$$\omega_s = 2l\omega_{m,s}. \quad (84)$$

The Dirac delta at $\omega = 0$ on the right hand side of Eq. (81) corresponds to the carrier optical frequency, and the Dirac deltas at $\omega = \pm\omega_s$ to sidebands which are created as the particle rotating at the frequency $\omega_{m,s}$ encounters $2l$ optical lattice sites. These sidebands fundamentally arise from the rotational Doppler shift [55, 56] imprinted on the cavity photons by the mechanical motion. The rotation frequency peak at ω_s can thus be recovered by homodyning (i.e. interfering with a piece which was split off from the probe beam before it enters the cavity) the probe beam $LG_{\pm l}$ once it has exited the cavity [11]. An investigation into the nonlinear regime of high probe power shows that the measurement accuracy eventually degrades as shown in Fig. 10. At very high powers, the nanoparticle is simply trapped in one of probe lattice wells.

While the description above provides some initial exploration of the coupling between optical and particle OAM, much remains to be accomplished in this area. Particularly, the quantum regime needs to be explored. A situation where the quantum regime could be relevant is when the dielectric nanoparticle is replaced by a single atom.

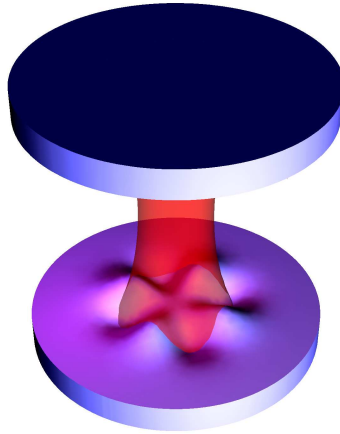


Figure 11. (Color online) The system described in Section 5.3. Surface acoustic waves on the lower mirror couple to the optical mode supported by the cavity. Reproduced with permission from [87].

No experiment to date has been able to detect or manipulate the center-of-mass angular momentum of a single atom, see Section 6.3 below. This is in contrast to other degrees of freedom, such as electronic and translational center-of-mass for which fine control has been established at the single atom level [115, 116, 117]. Such control is desirable for rotational degrees of freedom from a fundamental perspective, but also for applications such as quantum information processing [69, 71].

5.3. Surface Acoustic Waves

In this section we will consider the coupling of Laguerre-Gaussian optical cavity modes with acoustic waves on the surface of a highly reflective mirror, see Fig. 11. This mirror is one of two that make up a Fabry-Perot, of the kind described in Section 2.3. The acoustic excitations manifest as vibrations of the mirror surface along the cavity axis. Importantly, the vibrational modes also carry azimuthal structure. To our knowledge, Briant et al. were the first to experimentally demonstrate that standard optomechanical physics of Eq. (41) could be realized by such vibrational modes, which do not involve any global motion of the mirror [118]. They were able to detect the azimuthal profile of each mode by scanning a sharply focused Gaussian beam, whose waist was much smaller than that of the surface acoustic mode, across the mirror surface and following the resulting phase shifts in the reflected cavity beam.

The experimentally acquired mechanical mode vibrational frequencies and spatial mode profiles could be fit well by an analytical theory in the limit where the radius of curvature of the mirror was much larger than its thickness. In this limit, the elasticity equation, which determines the mechanical modes, took a form identical to the *optical* paraxial equation. This implied that each mechanical mode could be characterized as

a Laguerre-Gaussian mode, as confirmed by the experimental data. In this case the mechanical phonons of the mirror surface acoustic field may be thought of as harmonic oscillator quanta which carry OAM transverse to their direction of oscillation. They are therefore analogous to Laguerre-Gauss photons of the electromagnetic field which are also quanta of a harmonic oscillator, and also carry OAM in the same manner.

The work of Briant et al. was extended in [87] which subsequently explored the coupling of the mentioned mechanical Laguerre-Gaussian modes (with indices l' and p') to optical cavity (with indices l and p) Laguerre-Gaussian modes. The interaction Hamiltonian in this case is found by expanding the acoustic as well as optical fields in terms of Laguerre-Gaussian modes [analogous to Eqs. (17) and (18) which expand the field in terms of sines and cosines], and yields

$$H_{\text{SAW}} = \hbar g_{\text{SAW}} a^\dagger a (c + c^\dagger), \quad (85)$$

which is exactly of the same form as Eq. (36), except for the coupling constant

$$g_{\text{SAW}} = g' \delta_{|l'|, 2|l|} \xi_{lpp'}, \quad (86)$$

where g' is given in Eq. (42) and the full expression for $\xi_{lpp'}$ has not been reproduced here as it is quite lengthy. From the Kronecker delta in Eq. (86) we can deduce the OAM selection rule

$$|l'| = 2|l|, \quad (87)$$

for $l, l' \neq 0$. The factor of two in Eq. (87) may be traced back to the fact that the optomechanical interaction is bilinear in the optical field, but only linear in the acoustic field. The selection rule of Eq. (87) provides a path for targeting specific mechanical modes. In the original proposal this selectivity was exploited for storing photonic OAM in mechanical vibrational modes [87]. However, there is no analogous rigorous selection rule for p and p' , only simply varying degrees of overlap between modes with various radial numbers, described by the factor $\xi_{lpp'}$. We note that for this optomechanical platform, angular momentum is carried and exchanged in a parametric way, and is not a dynamical variable with its own time evolution.

6. Cavityless optomechanics

In this section we briefly consider the interaction of mechanical degrees of freedom with electromagnetic modes which are not confined in a resonator, but propagate freely in space. Such configurations constitute a rapidly growing class of optomechanical systems [119, 120]. Below we will describe linear vibrational motion and then move on to torsional and then finally rotational motion.

6.1. Vibrational motion

A typical configuration consists of a harmonically oscillating subwavelength dielectric particle trapped optically at the focus of a freely propagating Gaussian optical beam, see

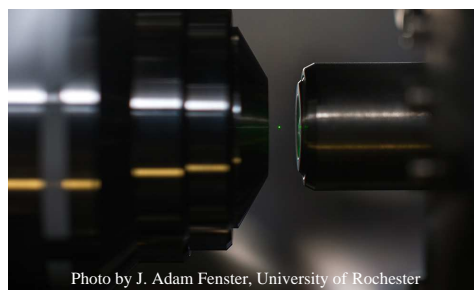


Figure 12. (Color online) The system described in Section 6.1. An optically levitated nanoparticle scattering light from the 1064nm trapping laser. Reproduced with permission from Prof. A. N. Vamivakas.

Fig. 12. When this configuration is placed inside a liquid medium, it is usually referred to as an ‘optical tweezer’ [79]. In the present case we will consider optical trapping in vacuum only. Photons scattered by the trapped particle are used as a probe to detect its motion. At low background pressures, the particle motion is ballistic and simple harmonic to a very good approximation. The frequency of oscillation along each spatial direction is set by the intensity of the trapping beam.

An example of an optomechanical effect in this system is cooling of the oscillator motion, using a technique different from that described in Section 2.3. Cooling can be achieved by making the trapping beam intensity (and therefore the mechanical trap frequency) higher when the particle is moving away from the center of the trap, and lower when it is moving towards. Using such a technique, cooling has been implemented from 300K (room temperature) to 50mK [121]. The system can also be used as a thermometer [29], as a force sensor [26], and can carry other spin-like degrees of freedom [122]. Theoretical proposals exist for creating macroscopic superpositions in such systems [123, 124].

6.2. Torsional motion

Exchange of angular momentum between an optical field and a torsional mechanical oscillator in free space was first seen in a classic experiment by Beth [44]. By detecting the rotation of a quarter-wave plate suspended as a torsional oscillator due to the change in handedness of polarized light passing through it, Beth was in fact able to experimentally show for the first time that light possesses angular momentum. The experiment has been repeated in modern times in the optical [45] as well as microwave [125] domains.

6.3. Rotational motion

In this section we describe several examples of the coupling of light carrying angular momentum to free mechanical rotation.

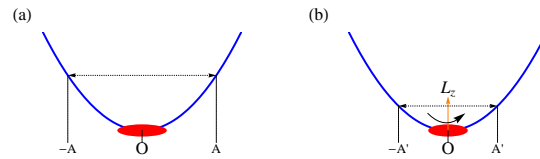


Figure 13. (Color online) The system described in Section 6.3.2. (a) shows a trapped asymmetric particle executing simple harmonic motion with amplitude A (b) shows the same particle spinning at a constant angular momentum L_z about an axis transverse to the vibrational motion. The conservation of angular momentum results in a reduced amplitude of motion $A' < A$, which may be thought of as gyroscopic cooling of vibration [50].

6.3.1. Spinning graphene Charged flakes of graphene have been confined in an electrostatic trap under vacuum [126]. The linear motion is to a good approximation harmonic along all three spatial directions. In addition, it was found that when the flake was irradiated with circularly polarized light, it spun at about 10 MHz. The mechanism for angular momentum transfer was light absorption.

6.3.2. Optomechanical gyroscope Optically trapped particles can exhibit interesting interplay between vibrational and rotational degrees of freedom, as demonstrated using an optomechanical gyroscope [50]. The trapped nanoparticle in this case was slightly anisotropic in shape, and the linear degrees of freedom were harmonic, as in the examples above. As in the case of graphene, a circularly polarized light beam set the particle in rotation. An interesting effect was then demonstrated that involved both vibration and rotation, as shown in Fig. 13. In the absence of rotation, the particle oscillated with a certain amplitude along each axis, as shown in Fig. 13 (a). In the presence of rotation, however, the particle became resistant to changing the direction of its angular momentum, as for any spinning top. This led to a decrease in the oscillation amplitude of the vibrational particle motion, as shown in Fig. 13(b). This effect corresponds to ‘gyroscopic cooling’ of vibrational motion, distinct from resonator-based (Section 2.3) and feedback (Section 6.1) cooling. In the experiment cooling of other rotational modes was also observed.

6.3.3. Rotating atoms, molecules and electrons For completeness we mention that there is a sizable literature associated with the transfer of optical angular momentum to the center-of-mass motion of hot [127], cold [128, 129, 130, 131, 132, 133, 134, 135] and degenerate [52, 53, 54, 136, 137, 138, 139, 140, 141, 142, 143, 144, 145] atoms, molecules [146], and electrons [147]. There are many phenomena of interest in this category including vortices, persistent currents, spin textures, and optical centrifuges. We will not describe these works in detail here, since they go back several years, if not decades.

7. Conclusion and outlook

In this tutorial, we have presented some introductory examples of the rich optomechanics arising from the exchange of angular momentum between light and matter. We have attempted to relate the relevant theoretical tools to the earlier work on vibrational optomechanics, while trying to present a useful variety of experimental platforms on which the theory could be realized. We therefore hope our exposition will be of relevance to theorists as well as experimentalists.

8. Acknowledgements

We are grateful to B. Zwickl, M. Vengalattore, S. Agarwal and B. Rodenburg for useful discussions. We would like to thank the Research Corporation for Science Advancement (Award No. 20966) and the National Science Foundation (Award No. 1454931) for Support.

- [1] Karrai K 2006 A Cooling Light Breeze *Nature* **444** 41
- [2] Kippenberg T J and Vahala K 2008 Cavity Optomechanics: Back-Action at the Mesoscale *Science* **321** 1172
- [3] Marquardt F, Clerk A A and Girvin S M 2008 Quantum theory of optomechanical cooling *J. Mod. Opt.* **55** 3329
- [4] Marquardt F and Girvin S 2009 Optomechanics *Physics* **2** 40
- [5] Clerk A A, Devoret M H, Girvin S M, Marquardt F and Schoelkopf R J 2010 Introduction to Quantum Noise, Measurement and Amplification *Physics* **2** 40
- [6] Aspelmeyer M, Groblacher S, Hammerer K and Keisel N 2010 Quantum optomechanics - throwing a glance *J. Opt. Soc. Am. B* **27** 0740
- [7] McClelland D E, Mavalvala N, Chen Y, and Schnabel R 2011 Advanced interferometry, quantum optics and optomechanics in gravitational wave detectors, *Laser Phot. Rev.* **5**, 677
- [8] Regal C A and Lehnert K W 2011 From cavity electromechanics to cavity optomechanics *J. of Phys.: Conf. Series* **264**, 012025
- [9] Aspelmeyer M, Meystre P and Schwab K 2012 Quantum optomechanics *Physics Today* **65**, 29
- [10] Meystre P 2013 A short walk through quantum optomechanics *Ann. der Physik* **525** 215
- [11] Aspelmeyer M, Kippenberg T J, and Marquardt F 2014 Cavity optomechanics *Rev. Mod. Phys.* **86** 1391
- [12] Metcalfe M, 2014 Applications of cavity optomechanics *Appl. Phys. Rev.* **1** 031105
- [13] Debnath K, and Bhattacharjee A B 2014 Cavity quantum electrodynamics of ultracold atoms in optical and optomechanical cavities arxiv:14110248v1
- [14] Chan J, Mayer Alegre T P, Safavi-Naeini A H, Hill J T, Krause A, Grblacher S, Aspelmeyer M and Painter O 2011 Laser cooling of a nanomechanical oscillator into its quantum ground state *Nature* **478** 89
- [15] Nimmrichter S, Hornberger K, and Hammerer K 2014 Optomechanical Sensing of Spontaneous Wave-Function Collapse *Phys. Rev. Lett.* **113** 020405
- [16] Diosi L 2015 Testing Spontaneous Wave-Function Collapse Models on Classical Mechanical Oscillators *Phys. Rev. Lett.* **114** 050403
- [17] Marshall W, Simon C, Penrose R, and Bouwmeester D 2003 Towards Quantum Superpositions of a Mirror *Phys. Rev. Lett.* **91** 130401
- [18] Romero-Isart O, Pflanzner A C, Blaser F, Kaltenbaek R, Kiesel N, Aspelmeyer M, and Cirac J I 2011 Large Quantum Superpositions and Interference of Massive Nanometer-Sized Objects *Phys. Rev. Lett.* **107** 020405

- [19] Pepper B, Ghobadi R, Jeffrey E, Simon C, and Bouwmeester D 2012 Optomechanical Superpositions via Nested Interferometry *Phys. Rev. Lett.* **109** 023601
- [20] Lee K C, Sprague M R, Sussman B J, Nunn J, Langford N K, Jin X M, Champion T, Michelberger P, Reim K F, England D, Jaksch D and Walmsley I A 2011 Entangling Macroscopic Diamonds at Room Temperature *Science* **334** 1253
- [21] Palomaki T A, Teufel J D, Simmonds R W, and Lehnert K W 2013 Entangling Mechanical Motion with Microwave Fields *Science* **342** 710
- [22] Purdy T P, Peterson R W, and Regal C A 2013 Observation of Radiation Pressure Shot Noise on a Macroscopic Object *Science* **339** 801
- [23] Pikovski I, Vanner M R, Aspelmeyer M, Kim M S, and Brukner C 2012 Probing Planck-scale physics with quantum optics *Nat. Phys.* **8** 393
- [24] Hertzberg J B, Rocheleau T, Ndukum T, Savva M, Clerk A A, and Schwab K C 2010 Back-action Evading Measurements of Nanomechanical Motion *Nat. Phys.* **6** 213
- [25] Schreppler S, Spethmann N, Brahms N, Botter T, Barrios M, and Stamper-Kurn D M 2014 Optically Measuring Force near the Standard Quantum Limit *Science* **344** 1486
- [26] Moore D C, Rider A D, and Gratta G 2014 Search for Millicharged Particles Using Optically Levitated Microspheres *Phys. Rev. Lett.* **113** 251801
- [27] Clerk A A, Marquardt F, and Harris J G E, 2010 Quantum Measurement of Phonon Shot Noise *Phys. Rev. Lett.* **104** 213603
- [28] Cohen J D, Meenehan S M, MacCabe G S, Groeblacher S, Safavi-Naeini A H, Marsili F, Shaw M D, and Painter O 2015 Phonon counting and intensity interferometry of a nanomechanical resonator *Nature* **520** 522
- [29] J. Millen, T. Deesuwana, P. Barker, and J. Anders 2014 Nanoscale temperature measurements using non-equilibrium Brownian dynamics of a levitated nanosphere *Nat. Nano.* **9** 425
- [30] Krause A G, Winger M, Blasius T D, Lin Q, and Painter O 2012 A high-resolution microchip optomechanical accelerometer *Nat. Phot.* **6** 768
- [31] Forstner S, Prams S, Knittel J, van Ooijen E D, Swaim J D, Harris G I, Szorkovszky A, Bowen W. P., and Rubinsztein-Dunlop H 2012 Cavity Optomechanical Magnetometer *Phys. Rev. Lett.* **108** 120801
- [32] Allen L, Barnett S M, and Padgett M J, Editors 2003 *Optical Angular Momentum*, (United States: Institute of Physics Publishing)
- [33] Kolobov M, Editor 2007 *Quantum Imaging*, (Germany: Springer)
- [34] Bekshaev A, Soskin M and Vasnetsov M, 2008 *Paraxial Light Beams With Angular Momentum*, (New York: Nova Science Publishers)
- [35] Torres J P and Torner L, Editors 2011 *Twisted Photons: Applications of Light with Orbital Angular Momentum*, (Germany: Wiley-VCH)
- [36] Andrews D L and Babiker M L, Editors, 2012 *The Angular Momentum of Light*, (United Kingdom: Cambridge University Press)
- [37] Andrews D L, 2012 *Structured Light and Its Applications: An Introduction to Phase-Structured Beams and Nanoscale Optical Forces*, (United States: Academic Press)
- [38] Allen L, Padgett M and Babiker M, 1999 The Orbital Angular Momentum of Light *Prog. Opt.* **39** 291
- [39] Loudon R, 1999 Theory of the forces exerted by Laguerre-Gaussian light beams on dielectrics *Phys. Rev. A* **68** 013806
- [40] Padgett M, Courtial J and Allen L, 2004 Light's Orbital Angular Momentum *Phys. Today* **57** 35
- [41] Franke-Arnold S, Allen L and Padgett M, 2008 Advances in Optical Angular Momentum *Laser Photon. Rev.* **2** 299
- [42] Yao A M and Padgett M J, 2011 Orbital Angular Momentum: origins, behavior and applications *Ad. Opt. Phot.* **3** 161
- [43] Bliokh K Y, Ostrovskaya E A, Alonso M A, Rodriguez-Herrera O G, Lara D and Dainty C, 2011 Spin-to-orbital angular momentum conversion in focusing, scattering, and imaging systems *Opt.*

- Exp.* **19** 26132
- [44] Beth, R A 1936 Mechanical Detection and Measurement of the Angular Momentum of Light *Phys. Rev.* **50** 115
- [45] Moothoo D N, Arlt J, Conroy R S, Akerboom F, Voit A, and Dholakia K 2001 Beths experiment using optical tweezers *Am. J. Phys.* **69** 271
- [46] Allen L, Beijersbergen M W, Spreeuw R J C and Woerdman J P, 1992 Orbital angular momentum of light and the transformation of Laguerre-Gaussian laser modes *Phys. Rev. A* **45** 8185
- [47] Galvez E J, Coyle L E, Johnson E and Reschovsky B J, 2011 Interferometric measurement of the helical mode of a single photon *N. J. Phys.* **13** 053017
- [48] He H, Friese M, Heckenberg N R and Rubinsztein-Dunlop H 2001 Direct observation of transfer of angular momentum to absorptive particles from a laser beam with a phase singularity *Phys. Rev. Lett.* **75** 826
- [49] Simpson N, Dholakia K, Allen L, and Padgett M 1997 Mechanical equivalence of spin and orbital angular momentum of light: an optical spanner *Opt. Lett.* **22** 52
- [50] Yoshihiko A, Mazilu M and Dholakia K 2013 Laser-induced rotation and cooling of a trapped microgyroscope in vacuum *Nat. Comm.* **3374**, 1
- [51] Piccirillo B, Toscano C, Vetrano F and Santamato E 2001 Orbital and Spin Photon Angular Momentum Transfer in Liquid Crystals *Phys. Rev. Lett.* **86** 2285
- [52] Andersen M, Ryu C, Clade P, Natarajan V, Vaziri A, Helmerson K and Phillips W D 2006 Quantized Rotation of Atoms from Photons with Orbital Angular Momentum *Phys. Rev. Lett.* **97** 170406
- [53] Ryu C, Andersen M F, Clade P, Natarajan V, Helmerson K and Phillips W D 2007 Observation of Persistent Flow of a Bose-Einstein Condensate in a Toroidal Trap *Phys. Rev. Lett.* **99** 260401
- [54] Wright K C, Leslie L S and Bigelow N P 2008 Optical control of the internal and external angular momentum of a Bose-Einstein condensate *Phys. Rev. A* **77** 041601(R)
- [55] Bialynicki-Birula I and Bialynicki-Birula Z 1997 Rotational Frequency Shift *Phys. Rev. Lett.* **78** 2539
- [56] Barreiro S, Tabosa J W R, Failache H and Lezama A 2006 Spectroscopic Observation of the Rotational Doppler Effect *Phys. Rev. Lett.* **97** 113601
- [57] Lavery M P J, Speirits F C, Barnett S M and Padgett M J, 2013 Detection of a Spinning Object Using Lights Orbital Angular Momentum *Science* **341**, 537
- [58] Phillips D B, Lee M P, Speirits F C, Barnett S M, Simpson S H, Lavery M P J, Padgett M J and Gibson G M, 2014 Rotational Doppler velocimetry to probe the angular velocity of spinning microparticles *Phys. Rev. A* **90**, 011801(R)
- [59] Lavery M P J, Barnett S M, Speirits F C and Padgett M J, 2014 Observation of the rotational Doppler shift of a white-light, orbital-angular-momentum-carrying beam backscattered from a rotating body *Optica* **1**, 2334
- [60] Korech O, Steinitz U, Gordon R J, Averbukh I. S. and Prior Y, 2007 Observing molecular spinning via the rotational Doppler effect *Nat. Phot.* **7**, 3711
- [61] Mair A, Vaziri A, Weihs G and Zeilinger A, 2001 Entanglement of the orbital angular momentum states of photons *Nature* **412** 313
- [62] Molina-Terriza G, Torres J P and Torner L, 2001 Management of the Angular Momentum of Light: Preparation of Photons in Multidimensional Vector States of Angular Momentum *Phys. Rev. Lett.* **88** 013601
- [63] Collins D, Gisin N, Linden N, Massar S and Popescu S, 2002 Bell Inequalities for Arbitrarily High-Dimensional Systems *Phys. Rev. Lett.* **88** 040404
- [64] Cerf N, Bourennane M, Karlsson A and Gisin N, 2002 Security of Quantum Key Distribution Using d -Level Systems *Phys. Rev. Lett.* **88** 127902
- [65] Molina-Terriza G, Torres J P and Torner L, 2007 Twisted Photons *Nat. Phys.* **3**, 305
- [66] Gbur G and Tyson R K, 2008 Vortex beam propagation through atmospheric turbulence and topological charge conservation *J. Opt. Soc. Am. (B)* **25**, 225

- [67] Lanyon B P, Barbieri M, Almeida M P, Jennewein T, Ralph T C, Resch K J, Pryde G J, O'Brien J L, Gilchrist A and White A G, 2009 Simplifying quantum logic using higher-dimensional Hilbert spaces *Nat. Phys.* **7** 134
- [68] Giovannini D, Nagali E, Marucci L and Sciarrino F, 2011 Resilience of orbital-angular-momentum photonic qubits and effects on hybrid entanglement *Phys. Rev. A* **83** 042338
- [69] Fickler R, Lapkiewicz R, Plick W N, Krenn M, Schaeff C, Ramelow S and Zeilinger A, 2012 Quantum Entanglement of High Angular Momenta *Science* **338** 640
- [70] Garcia-Escartin J C and Chamorro-Posada P, 2012 Quantum computer networks with the orbital angular momentum of light *Phys. Rev. A* **86** 032334
- [71] Mirhosseini M, Magaa-Loaiza O S, OSullivan M N, Rodenburg B, Malik M, Lavery M P J, Padgett M J, Gauthier D J and Boyd R W, 2015 High-dimensional quantum cryptography with twisted light *N. J. Phys.* **17**, 033033
- [72] Berry M V and Nye J F 1974 Dislocations in Wave Trains *Proc. Roy. Soc. Lond. Ser. A* **336**, 165
- [73] Mansuripur M and Wright E M 1999 Optical Vortices *Opt. Phot. News* **February**, 40
- [74] Lee J H, Foo G, Johnson E G, and Swartzlander Jr G A, 2009 Experimental verification of an optical vortex coronagraph *Phys. Rev. Lett.* **97**, 053901
- [75] Dennis M, O'Holleran K and Dennis M 2009 Singular Optics: optical vortices and polarization singularities *Prog. Opt.* **53**, 293
- [76] Padgett M and Allen L 1997 Optical tweezers and spanners *Phys. World* **10**, 35
- [77] Dholakia K, Spalding G and Macdonald M 2002 Optical tweezers: the next generation *Phy. World* **2** 31
- [78] Grier D 2003 A revolution in optical manipulation *Nature* **424**, 810
- [79] Moffitt J R, Chemla Y R, Smith S B and Bustamante C, 2008 Recent Advances in Optical Tweezers *Ann. Rev. of Biochem.* **77**, 205
- [80] Tittonen I, Breitenbach G, Kalkbrenner T, Muller T, Conradt R, Schiller S, Steinsland E, Blanc N and de Rooij N F, 1999 Interferometric measurements of the position of a macroscopic body: towards the observation of quantum limits *Phys. Rev. A* **59**, 1038
- [81] Mueller F, Huegel S and Wang L J, 2009 Optomechanical stochastic resonance in a macroscopic torsion oscillator *Phys. Rev. A* **79**, 031804
- [82] Wang Q L, Yeh H C, Zhou Z B and Luo J, 2009 Improving the sensitivity of a torsion pendulum by using an optical spring method *Phys. Rev. A* **80**, 043811
- [83] Kim P H, Doolin C, Hauer B D, MacDonald A J R, Freeman M R, Barclay P E and Davis J P, 2013 Nanoscale torsional optomechanics *Appl. Phys. Lett.* **102**, 053102
- [84] Coulomb C A, 1788 Premier Mmoire sur llectricit et le Magntisme. Construction et usage dune Balance lectrique, fonde sur la proprit quont les fils de mtal davoit une force de raction de torsion proportionnelle langle de Torsion *Mmoires de lAcadmie Royale des Sciences* **1788**, 569
- [85] Cavendish H, 2013 Experiments to determine the density of the earth *Phil. Trans.* **17**, 469
- [86] Sakurai J J, 2010 *Modern Quantum Mechanics*, (United States: Addison-Wesley)
- [87] Shi H and Bhattacharya M 2013 Mechanical memory for photons with optical angular momentum *J. Phys. B* **46**, 151001
- [88] Jha A K, Agarwal G S and Boyd R W 2011 Supersensitive measurement of angular displacements using entangled photons *83* **83**, 053829
- [89] Mooij J E, Orlando T P, Levitov L, Tian L, van der Wal C H and Lloyd S, 1999 Josephson persistent-current qubit *Science* **285**, 1036
- [90] Bhattacharya M, Shi H and Preble S 2013 Coupled second quantized oscillators *Am. J. Phys.* **81** 267
- [91] Genes C, Vitali D, Tombesi P, Gigan S and Aspelmeyer M 2008 Ground-state cooling of a micromechanical oscillator: Comparing cold damping and cavity-assisted cooling schemes *Phys. Rev. A* **77** 033804
- [92] Gerry C C and Knight P L, *Introductory Quantum Optics*, (United Kingdom: Cambridge University Press)

- [93] Law C K 1995 Interaction between a moving mirror and radiation pressure: A Hamiltonian formulation *Phys. Rev. A* **51** 2537
- [94] Galvez E J 2006 Gaussian beams in the optics course *Am. J. Phys.* **74** 355
- [95] Karimi E, Boyd R W, de la Hoz P, de Guise H, Rehacek J, Hradil Z, Aiello A, Leuchs G and Sanchez-Soto L. L. 2014 Radial quantum number of Laguerre-Gauss modes *Phys. Rev. A* **89** 063813
- [96] Bhattacharya M and Meystre P 2007 Using a Laguerre-Gaussian beam to trap and cool the rotational motion of a mirror *Phys. Rev. Lett.* **99** 153603
- [97] Fickler R, Lapkiewicz R, Plick W N, Krenn M, Schaeff C, Ramelow S and Zeilinger A 2012 *Science* **338** 640
- [98] Kudryashov A V and Paxton A H 2000 *Laser Resonators III*, (SPIE, Bellingham, Washington)
- [99] Eggleston M, Godat T, Munro E, Alonso M A, Shi H and Bhattacharya M 2007 Ray transfer matrix for a spiral phase plate *J. Opt. Soc. Am. A* **20** 2526
- [100] Rumala Y 2015 Wave transfer matrix for a spiral phase plate *App. Opt.* **54** 4395
- [101] Oron R, Davidson N, Friesem A A and Hasman E 2001 Transverse mode shaping and selection in laser resonators *Prog. Opt.* **42** 325
- [102] Romero-Isart O, Juan M L, Quidant R and Cirac J I 2010 Toward quantum superposition of living organisms *N. J. Phys.* **12** 033015
- [103] Shi H and Bhattacharya M 2013 Coupling a small torsional oscillator to large optical angular momentum *J. Mod. Opt.* **5** 382
- [104] Novotny L and Hecht B, 2012 *Principles of Nano-Optics*, (United Kingdom: Cambridge University Press)
- [105] Higurashi E, Ukita H, Tanaka H, and Ohguchi O 1994 Optically induced rotation of anisotropic micro-objects fabricated by surface micromachining *Appl. Phys. Lett.* **64** 2209
- [106] Kuhn S, Asenbaum P, Kosloff A, Sclafani M, Stickler B A, Nimmrichter S, Hornberger K, Cheshnovsky O, Patolsky F and Arndt M 2015 Cavity-Assisted Manipulation of Freely Rotating Silicon Nanorods in High Vacuum *Nano Lett.* **15** 5604
- [107] Lechner W, Habraken S J M, Kiesel N, Aspelmeyer M, and Zoller P 2013 Cavity Optomechanics of Levitated Nanodumbbells: Nonequilibrium Phases and Self-Assembly *Phys. Rev. Lett.* **110** 143604
- [108] Zhang X, Tomes M, Carmon T 2011 Precession Optomechanics *Op. Ex.* **19** 9066
- [109] Rubin J T and Deych L I 2011 Optical forces due to spherical microresonators and their manifestation in optically induced orbital motion of nanoparticles *Phys. Rev. A* **84** 023844
- [110] Arnold S, Keng D, Shopova S I, Holler S, Zurawsky W and Vollmer F 2009 Whispering gallery mode carousel a photonic mechanism for enhanced nanoparticle detection in biosensing *Opt. Express* **17** 6230
- [111] Cheung H K and Law C K 2012 Optomechanical coupling between a moving dielectric sphere and radiation fields: A Lagrangian-Hamiltonian formalism *Phys. Rev. A* **86** 033807
- [112] Bhattacharya M 2015 Rotational cavity optomechanics *J. Opt. Soc. Am.* **32** B55
- [113] Carruthers P and Nieto M M 1968 Phase and Angle Variables in Quantum Mechanics *Rev. Mod. Phys.* **40** 411
- [114] Sacconi L, Romano G, Ballerini R, Capitanio M, De Pas M, Giuntini M, Dunlap D, Finzi L, and Pavone F S 2001 Three-dimensional magneto-optic trap for micro-object manipulation *Opt. Lett.* **26** 1359
- [115] Meschede D and Rauschenbeutel A 2006 Manipulating single atoms *Ad. At. Mol. Opt. Phys.* **53** 75
- [116] Wineland D J 2006 Nobel Lecture: Superposition, entanglement, and raising Schrödinger's cat *Rev. Mod. Phys.* **85** 1103
- [117] Wieman C E, Pritchard D E and Wineland D J 1999 Atom cooling, trapping, and quantum manipulation *Rev. Mod. Phys.* **71** 253
- [118] Briant T, Cohadon P F, Heidmann A And Pinard M 2003 Optomechanical characterization of

- acoustic modes in a mirror *Phys. Rev. A* **68** 033823
- [119] Z.-Q. Yin, A. A. Geraci, T. Li 2012 Optomechanics of Levitated Dielectric Particles *Int. J. Mod. Phys.* **27** 1330018
- [120] L. P. Neukirch and A. N. Vamivakas 2015 Nano-optomechanics with levitated nanoparticles *Cont. Phys.* **56** 48
- [121] Gieseler J, Deutsch B, Quidant R and Novotny L 2012 Subkelvin Parametric Feedback Cooling of a Laser-Trapped Nanoparticle *Phys. Rev. Lett.* **109** 103603
- [122] Neukirch L P, von Haartman E, Rosenholm J M and Nick Vamivakas A. N. 2015 Multi-dimensional single-spin nano-optomechanics with a levitated nanodiamond *Nat. Photonics* **9** 653
- [123] Scala M, Kim M S, Morley G W, Barker P F and Bose S 2015 Matter-wave interferometry of a levitated thermal nano-oscillator induced and probed by a spin *Phys. Rev. Lett.* **111** 180403
- [124] Yin Z Q, Li T, Zhang X and Duan L M 2013 Large quantum superpositions of a levitated nanodiamond through spin-optomechanical coupling *Phys. Rev. A* **88** 033614
- [125] Emile O, Brousseau C, Emile J, Niemiec R, Madhjoubi K and Thide B 2014 Electromagnetically Induced Torque on a Large Ring in the Microwave Range *Phys. Rev. Lett.* **112** 053902
- [126] Kane B E 2010 Levitated spinning graphene flakes in an electric quadrupole ion trap *Phys. Rev. B* **82** 115441
- [127] Chen Q F, Shi B S, Zhang Y S and Guo G C 2008 Entanglement of the orbital angular momentum states of the photon pairs generated in a hot atomic ensemble *Phys. Rev. A* **78** 053810
- [128] Tabosa J W R and Petrov D V 1999 Optical Pumping of Orbital Angular Momentum of Light in Cold Cesium Atoms *Phys. Rev. Lett.* **83** 4967
- [129] Muthukrishnan A and Stroud Jr C R 2002 Entanglement of internal and external angular momenta of a single atom *J. Opt. B: Quant. Semiclass. Opt* **4** S73
- [130] Inoue R, Kanai N, Yonehara T, Miyamoto Y, Koashi M and Kozuma M 2006 Entanglement of orbital angular momentum states between an ensemble of cold atoms and a photon *Phys. Rev. A* **74** 053809
- [131] Jiang W, Chen Q F, Zhang Y S and Guo G C 2006 Computation of topological charges of optical vortices via nondegenerate four-wave mixing *Phys. Rev. A* **74** 043811
- [132] Pugatch R, Shuker M, Firstenberg O, Ron A and Davidson N 2007 Topological Stability of Stored Optical Vortices *Phys. Rev. Lett.* **98** 203601
- [133] Moretti D, Felinto D and Tabosa J W R 2009 Collapses and revivals of stored orbital angular momentum of light in a cold-atom ensemble *Phys. Rev. A* **79** 023825
- [134] Inoue R, Yonhara T, Miyamoto Y, Koashi M and Kozuma M 2009 Measuring Qutrit-Qutrit Entanglement of Orbital Angular Momentum States of an Atomic Ensemble and a Photon *Phys. Rev. Lett.* **103** 110503
- [135] Veissier L, Nicolas A, Giner L, Maxein D, Sheremet A S, Giacobino E and Laurat J 2013 *Opt. Lett.* **38** 712
- [136] Marzlin K P, Zhang W and Wright E M 1997 Vortex Coupler for Atomic Bose-Einstein Condensates *Phys. Rev. Lett.* **79** 4728
- [137] Dum R, Cirac J I, Lewenstein M and Zoller P 1998 Creation of Dark Solitons and Vortices in Bose-Einstein Condensates *Phys. Rev. Lett.* **780** 2972
- [138] Nandi G, Walser R and Schleich W P 2004 Vortex creation in a trapped Bose-Einstein condensate by stimulated Raman adiabatic passage *Phys. Rev. A* **69** 063606
- [139] Dutton Z and Ruostekoski J 2004 Transfer and Storage of Vortex States in Light and Matter Waves *Phys. Rev. Lett.* **93** 193602
- [140] Kapale K T and Dowling J P 2005 Vortex Phase Qubit: Generating Arbitrary, Counterrotating, Coherent Superpositions in Bose-Einstein Condensates via Optical Angular Momentum Beams *Phys. Rev. Lett.* **95** 173601
- [141] Kanamoto R, Wright E M and Meystre P 2007 Quantum dynamics of Raman-coupled Bose-Einstein condensates using Laguerre-Gaussian beams *Phys. Rev. A* **75** 063623

- [142] Wright K C, Leslie L S, Hansen A and Bigelow N P 2009 Sculpting the Vortex State of a Spinor BEC *Phys. Rev. Lett.* **102** 030405
- [143] Leslie L S, Hansen A, Wright K C, Deutsch B M and Bigelow N P 2009 Creation and Detection of Skyrmions in a Bose-Einstein Condensate *Phys. Rev. Lett.* **103** 250401
- [144] Gullo N L, McEndoo S, Busch T and Paternostro M 2010 Vortex entanglement in Bose-Einstein condensates coupled to Laguerre-Gauss beams *Phys. Rev. A* **81** 053625
- [145] Beattie S, Moulder S, Fletcher R J and Hadzibabic Z 2013 Persistent Currents in Spinor Condensates *Phys. Rev. Lett.* **110** 025301
- [146] Korobenko A, Milner A A and Milner V 2014 Direct Observation, Study, and Control of Molecular Superrotors *Phys. Rev. Lett.* **112** 113004
- [147] Handali J, Shakya P and Barwick B 2015 Creating electron vortex beams with light *Opt. Exp.* **23** 5236